Biomedical Materials

PAPER

Analyses of the modulatory effects of antibacterial silver doped calcium phosphate-based ceramic nano-powder on proliferation, survival, and angiogenic capacity of different mammalian cells *in vitro*

R Beklem Bostancıoğlu[1], Ceren Peksen[2], Hatice Genc[1], Mevlüt Gürbüz[3], Filiz Bayrakçı Karel[4], A Savas Koparal[4], Aydin Dogan[5], Nusret Kose[6] and A Tansu Koparal[1]

[1] Department of Biology, Anadolu University, 26470 Eskisehir, Turkey
[2] Faculty of Fine Arts, Department of Ceramic and Glass, Ondokuz Mayis University, 55200 Samsun, Turkey
[3] Department of Mechanical Engineering, Ondokuz Mayıs University, 55139 Samsun, Turkey
[4] Department of Environmental Engineering, Anadolu University, 26555 Eskisehir, Turkey
[5] Department of Materials Science and Engineering, Anadolu University, 26555 Eskisehir, Turkey
[6] Faculty of Medicine, Department of Orthopedics and Traumatology, Eskisehir Osmangazi University, 26480 Eskisehir, Turkey

E-mail: beklemb@gmail.com

Keywords: silver, antibacterial, cytotoxicity, angiogenesis, hydroxyapatite, biocompatability, nanopowder

OPEN ACCESS

RECEIVED
22 June 2015

REVISED
23 June 2015

ACCEPTED FOR PUBLICATION
6 July 2015

PUBLISHED
26 August 2015

Abstract

In this study, the antibacterial, cytotoxic, and angiogenic activities of silver doped calcium phosphate-based inorganic powder (ABT or PAG) were systematically investigated. ABT powders containing varying silver content were fabricated using a wet chemical manufacturing method. Antibacterial efficiencies of the ABT powders were investigated using a standard test with indicator bacteria and yeast. The cytotoxic effects of ABT on three different fibroblast cells and human umbilical vein endothelial cells (HUVECs) were assessed using MTT assay. ABT powder exhibits concentration-related cytotoxicity characteristics. Apoptotic activity, attachment capability, and wound healing effects were examined on fibroblasts. The angiogenic activity of ABT was investigated by tube formation assay in HUVECs; 10 μg ml^{-1} and 100 μg ml^{-1} concentrations of the highest metal ion content of ABT did not disrupt the tube formation of HUVECs. All these tests showed that ABT does not compromise the survival of the cells and might impose regeneration ability to various cell types. These results indicate that silver doped calcium phosphate-based inorganic powder with an optimal silver content has good potential for developing new biomaterials for implant applications.

1. Introduction

To avoid adverse health effects on patients, medical devices, along with their functional aspects, are biologically examined through biocompatibility testing, with the aim of identifying the variety of potential hazards and of making certain that these products do not have detrimental effects on patients [1]. Calcium phosphate-based biomaterials are mostly biocompatible, because calcium and phosphate are the main inorganic components of human bone [2]. All medical devices are required to be assessed via cytotoxicity measurements [3]. The tests that use cell cultures are rather advantageous because they provide an environment in which each biomaterial is open to individual evaluation in terms of cytotoxicity due to its influence on both cell growth and division [1, 4]. A vascular supply is vital for both the implantation of a new tissue into the body and for the survival of the growing cells within the implant [5, 6]. In addition to their role in the nutrient supply, newly formed blood vessels also help the transportation of macromolecules during bone repair and regeneration [7, 8].

For biomaterials, not only the biocompatibilities and their physical and chemical features but also the antibacterial properties are important [9]. Infection is a serious problem when biomaterials are implanted into the human body. It results from adherence and colonization of bacteria onto the biomaterials, and subsequently the patients develop serious complications, sometimes with lethal consequences [10]. Bactericidal activity of silver has been known for centuries. The evidence for silver's antibacterial properties' functionality in rendering water potable can be traced back to 1000 B.C. [11–13]. Silver compounds have also been used for medicinal purposes for centuries [14]. These compounds have been used for the treatments of tetanus and rheumatism in the 19th century, and for colds

and gonorrhea before the discovery of antibiotics in the early 20th century [15].

In the past decade, there have been many studies on silver-related biomaterials. Some of them show that silver has advantages; some of them show that silver has disadvantages. As matter of fact, silver has been a well-known antimicrobial metal ion for centuries. Just like any other chemical, silver must have a certain limit and application form in which we can use its antimicrobial efficacy without causing any toxic effect. One important thing that we should keep in mind is that the success of biomaterials as templates for tissue regeneration is mainly determined by their ability to rapidly vascularize and is a result of efficient delivery of requisite cellular nutrients during regeneration.

Silver and its compounds are well-known for their antibacterial properties in orthopedic and dental applications [16–18]. Ionization is required by elemental silver for antibacterial efficacy [19]. The highly reactive nature of silver ions reveals itself through readily binding to negatively charged components like proteins, RNA, DNA, and chloride ions. This characteristic is of crucial importance to its antibacterial mechanism, but due to its readily protein-bound nature it tends to complicate the delivery to the wound bed, because the complex wound fluid is full of proteins [20]. Silver delivery systems vary, namely the system that delivers silver from ionic compounds, such as silver calcium phosphate and silver chloride, and the system that delivers silver from metallic compounds, such as nanocrystalline silver [21, 22]. The effectiveness of silver against a wide range of microorganisms is a known fact. This range of effect extends to aerobic and anaerobic microorganisms, Gram-negative and Gram-positive bacteria, yeast, fungi, and viruses by binding to microbial DNA and to the sulfhydryl groups of the metabolic enzymes of the bacterial electron transport chain while also preventing bacterial reproduction [23]. Silver may also be of use as a prophylactic or a therapeutic agent for prohibition of colonization of organisms that hinder healing—those that contain antibiotic-resistant bacteria—at the wound site [24]. It has also been used as antibacterial wound dressings and therapeutics because of its acknowledged low toxicity [11].

In this study, the antibacterial, cytotoxic, proliferative, apoptotic, wound healing, and angiogenic activities of silver doped nano size calcium phosphate ceramic powders (ABT or PAG) were investigated systematically with various silver doping concentrations. Standard antimicrobial efficacy test with indicator bacteria and fungi was performed. MTT assays were used on V79 379A, NIH-3T3, TIG-114, and HUVEC lines to determine the effects of various silver doping concentrations on cytotoxicity. Additionally, the apoptotic activity (by DAPI and JC-1 staining), attachment capability (by F-actin staining), and the effects on wound healing were also evaluated on TIG-114 cells. The HUVEC cell line was used for *in vitro* angiogenesis assay. We demonstrated for the first time that silver doped calcium phosphate-based ceramic nano powder does not disturb angiogenesis and does not lead to apoptosis and demonstrates good regeneration ability by *in vitro*.

2. Materials and methods

2.1. Synthesis of powders

Silver ion incorporated antibacterial powders (ABT or PAG) were synthesized using wet chemical method. Ortho-phosphoric acid (99%), silver nitrate ($AgNO_3$, 99.0%), and calcium hydroxide ($Ca(OH)_2$, 96.0%) were all laboratory grade reagents and purchased from Sigma-Aldrich. Calcium hydroxide was mixed in pure water for 1 h. Dissolved silver nitrate in pure water was mixed with calcium hydroxide. Fully dissolved transparent silver nitride solution was added to calcium hydroxide solution drop by drop. The solution was stirred for approximately 2 h. Then, ortho-phosphoric acid diluted with pure water was added to the solution to control the pH of the solution to form a stoichiometric hydroxyapatite-based structure. Final pH has been set from 12.6 to 5.5 by ortho-phosphoric acid for all powder. The precipitate formed was sequentially filtered and dried at 80 °C. The crystal structure of the powders was monitored by x-ray difractometer (XRD, Rikagu Rint 2200) using the CuKα (1.542 A°) radiation and 2θ scan rate of 2° min^{-1} at 40 kV and 30 mA. The particle size distribution of the synthesized powders was measured using Malvern NanoZS device. The powder morphology and silver content were investigated by scanning electron microscopy (SEM), which has energy dispersive x-ray diffraction detector (Zeiss Evo 50EP and Zeiss Supra 50VP). Existence of silver ions in powder and primary particle size measurements were performed with transmission electron microscopy (TEM; Tecnai G2 F20 S-TWIN).

Before the *in vitro* assays five different ABT (00A, 05A, 10A, 20A, 35A) with various metal ion contents of powders were sterilized at 180 °C for 2 h.

Concentration amounts are listed below:

Abbreviations

00A	Calcium phosphate-based powder without Ag^+ ion (reference powder)
05A	Calcium phosphate-based powder containing 0.5 wt. % Ag^+ ion
10A	Calcium phosphate-based powder containing 1.0 wt. % Ag^+ ion
20A	Calcium phosphate-based powder containing 2.0 wt. % Ag^+ ion
35A	Calcium phosphate-based powder containing 3.5 wt. % Ag^+ ion

2.2. *In vitro* antibacterial activity

2.2.1. *Halo test method*

Halo test method was used to determine the antibacterial activity of powders. All glass ware were sterilized in an autoclave at 121 °C for 15 min before

performing the bacteria test. *Escherichia coli* colonies were cultivated in nutrient broth at 37 °C for 24 h in a shaking incubator. Formed colonies at the end of that period were diluted using dilution solutions such as saline. Following the dilution process, supplemented medium was put onto samples in Petri dishes to form a very thin layer just above the samples. *E.coli* from diluted solution was cultivated on the thin layer of supplemented medium (nutrient agar). Finally, Petri dishes were set in the incubator and bacteria growth was observed at various time intervals.

2.2.2. Agar dilution test method

Agar dilution method was performed using standard yeast (*Candida albicans* ATCC 10231) and bacteria (*Pseudomonas aeruginosa* ATCC 27853, *E. coli* ATCC 25922, *Staphylococcus aureus* ATCC 43300). Suspension of bacteria/yeast was diluted until the turbidity of 0.5 MacFarland turbidity standards was achieved. Powders with the final concentrations of 10%, 5%, 2.5%, 1.25%, 0.625%, and 0.313% were prepared in Mueller Hinton Agar by using the agar dilution method. Bacteria suspension having 0.5 MacFarland turbidity was added to this mixture in Petri dishes. The suspension was left to cool at room temperature. After solidification of agar, it was incubated at 37 °C, and at 24 and 48 h periods, bacteria colony formation was assessed. The results were confirmed using Gram dye.

2.3. *In vitro* cytotoxicity assay

2.3.1. Cells and cell culture

V79 379A (Chinese hamster lung fibroblast-like) and TIG-114 (normal human skin fibroblast) cell lines were obtained from JCRB, Osaka (IFO, Japan), and the NIH-3T3 (mouse embryo fibroblast) cell line was kindly provided by late Prof. Dr Yasuo Kitagawa (Nagoya University, Japan). V79 379A and NIH-3T3 cells were grown in Dulbecco's modified Eagle's medium (DMEM) containing 10% heat-inactivated fetal calf serum, 9.2% $NaHCO_3$, and 1% penicillin/streptomycin. TIG-114 cells were maintained in minimum essential medium containing 10% FBS, 1% penicillin-streptomycin. The HUVECs were purchased from the ATCC (American Type Cell Collection), which were incubated and grown in Nutrient Mixture F12 HAM medium supplemented with 20% heat-inactivated fetal calf serum, heparin (0.1 mg ml^{-1}), and endothelial cell growth supplement (ECGS; 0.05 mg ml^{-1}). Cells were cultured in a humidified atmosphere containing 5% CO_2 at 37 °C.

The five powders (00A, 05A, 10A, 20A, and 35A) were sterilized at 180 °C for 2 h. The growth inhibitory effects of the test compounds were measured using MTT (3-(4,5-dimethythiazol-2-yl)-2,5-diphenyl tetrazolium bromide) assay [25]. Cells were seeded in flat-bottomed 96-multiwell plates (Techno Plastic Products AG) and incubated at 37 °C for 24 h in a humidified atmosphere of 5% CO_2/95% O_2. Thereafter, old medium was replaced with fresh culture media supplemented with five different metal ion content of ABT at concentrations of 10 μg ml^{-1}, 100 μg ml^{-1}, and 1000 μg ml^{-1}. For references, old medium was replaced with fresh medium without powders. To test cytotoxicity, ABT of each concentration was cultured with V79 379A, NIH-3T3, TIG-114, and HUVECs for 24 h, 48 h, 72 h, and 96 h, respectively. During this period after each day, the medium was aspirated and 100 μl fresh medium containing 0.5 mg ml^{-1} MTT (Sigma) dissolved in phosphate-buffered saline (PBS) was added to culture wells. The plates with added MTT solution were then wrapped in aluminum foil and replaced in the 5% CO_2 incubator for 2 h. At the end of this period, the medium was removed and the formazan crystals formed by MTT metabolism were dissolved by addition of 100 μl DMSO to each well. The plates were gently mixed on a plate shaker approximately for 5 min, and their absorbance values were read at 570 nm with a microtiter plate reader (Bio-Tek, ELX808IU, USA). Every test concentration had the eight replicates per assay and every experiment was performed on at least three separate occasions.

The statistical software SPSS was used for the statistical analysis of assessment of the MTT assay. The data were evaluated using one-way ANOVA followed by the Tukey test. A value of $p < 0.05$ was considered as significant.

2.3.2. JC-1 staining

To explore whether the compounds induced apoptosis, we determined the mitochondrial membrane potential by morphological JC-1 staining. The loss of mitochondrial membrane potential is a hallmark for apoptosis. It is an early event coinciding with caspase activation. In healthy cells, red-orange fluorescence is attributable to a potential-dependent aggregation in the mitochondria even though green fluorescence reflecting the monomeric form JC-1 appeared in the cytosol. In apoptotic cells, green fluorescence dominates after mitochondrial membrane depolarization [26]. TIG-114 cells were seeded on 12-well plates at a concentration of 12×10^4. After 24 h cells were treated with different doses of powders and incubated 24 h. The treated cells were washed with PBS and incubated for 30 min in 10% MEM without phenol red containing JC-1 at a concentration of 2.5 g ml^{-1} and were observed by fluorescence microscopy.

2.3.3. DAPI staining

To determine whether there was degradation of DNA into fragments, DAPI staining, which is a DNA-staining agent and binds to grooves on the surface of the DNA helix, was performed [27]. TIG-114 cells were seeded on six-well plates at a density of 18×10^4 cells/well. After 24 h, old medium was replaced with fresh culture media supplemented with five different metal ion contents of ABT at concentrations of 10 µg ml^{-1}, 100 μg ml^{-1}, and 1000 μg ml^{-1}. Treated monolayers of cells, which were grown on glass coverslips (Marienfield, Germany), were

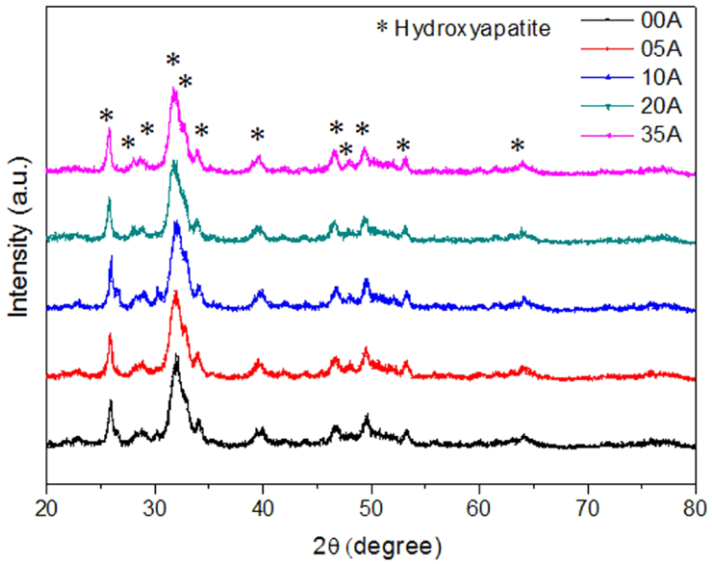

Figure 1. XRD analysis of the synthesized powders.

fixed with 3.7% (w/v) paraformaldehyde PBS (137 mM NaCl, 2.7 Mm KCl, 15 mM KH_2PO_4, 8 mM $NaHPO_4$; pH 7.3) for 15 min at 37 °C in the dark. Cells were rinsed with PBS. The results were acquired using Olympus fluorescence microscope (Olympus BX50 with U-UHK fluorescence attachment microscope).

2.3.4. F-actin staining (TRITC phalloidin)

The alterations in actin that provide the driving force during the process of cell migration via the formation of stress fibers, organization, and dynamics play an important role in apoptosis and also cell migration. The F-actin cytoskeleton was stained with fluorescent phalloidin using the method described by Rubin *et al* (1991) with slight modifications [28, 29]. Untreated control and ABT/00A, 15A, 20A, and 35A treated TIG-114 monolayers grown on glass coverslips (Marienfeld, Germany) were fixed in 3.7% (w/v) paraformaldehyde PBS for 15 min at 37 °C. The cells were then permeabilized with 0.5% Triton X-100 (v/v) in PBS for 5 min at 37 °C. Preparations were washed three times with PBS and cells were stained with 5 μg ml^{-1} tetramethylrhodamine B isothiocyanate (TRITC)-labelled phalloidin (Sigma) for 1 h at 37 °C. TIG-114 cells were rinsed with PBS; fluorescent images were acquired using an Olympus BX50 with U-UHK fluorescence attachment microscope.

2.3.5. Wound healing assay

For the process of angiogenesis to occur normally, both proliferation and migration are required. Migration is a key step required for angiogenesis. To assess the migratory response of fibroblast against these powders, a wound healing assay was performed. Cells were seeded into 12-well plates at a concentration of 12×10^4, after 24 h incubation a clear area was scraped in the monolayer with a narrow tip by applying suction, and cells were washed with the medium. Different concentrations of test compounds were administered and cells were incubated for another 24 h. After incubation cells were photographed (10X Olympus IX70).

2.3.6. In vitro capillary tube formation assay

In the later stages of angiogenesis, endothelial cells have to rearrange themselves into a tube to form a new small blood vessel. Thus, the endothelial cell tube formation assay used here is an *in vitro* model of this process. The matrigel tube formation assay was performed as previously described [30]. For this, HUVECs were starved by culturing in endothelial cell basal medium-2 with 2% FBS for 4 h. The serum starved cells were plated at the density of 4×10^4 cells/well on matrigel, which coated the wells of 96-well plates and were equilibrated with EBM-2 medium (containing powders when indicated). When cultured on matrigel, endothelial cells aligned themselves into a network structure within 12 h and the results were documented photographically using an inverted microscope (Olympus IX70) at 10X magnification.

3. Experimental results

The XRD analysis of the synthesized powders is displayed in figure 1. The crystal structure of synthesized powder is completely hydroxyapatite. The particle size distribution of ABT powders were analyzed after synthesis and ultrasonic homogenization.

The broad diffraction peaks of pure and silver doped hydroxyapatite in figure 1 mean that these materials contain nanosized apatite crystals. In addition, the diffraction patterns of hydroxyapatite are not affected by the addition of silver. There are no secondary or undesired crystalline phases related with silver in the XRD patterns, due to its low detection limit. The absence of these phases is due to the substitution of Ag

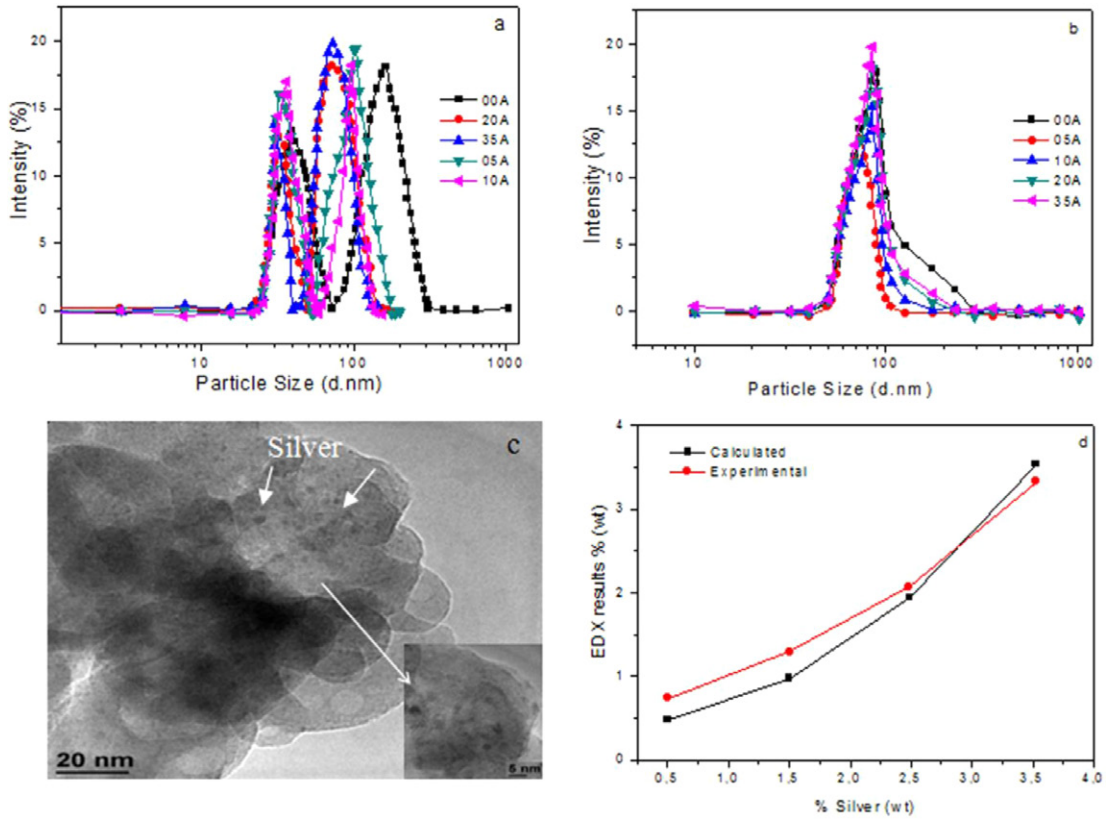

Figure 2. Particle size (a) and (b), TEM (for 35A) (c), and EDX (d) analysis of ABT powders.

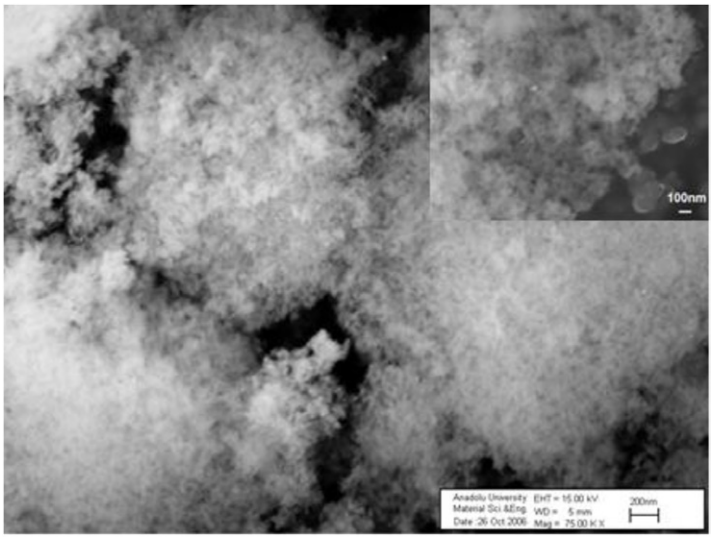

Figure 3. SEM micrographs of antibacterial ceramic nano-powders (75 000X).

with Ca without affecting the crystal structure of pure hydroxyapatite [31]. The published articles confirm XRD results of the current investigation. The reported silver doped hydroxyapatite articles give just pure hydroxyapatite phase from the XRD pattern due to the aforementioned reasons [32–34].

Figure 2(a) shows that the particles were highly agglomerated after synthesis. As shown in figure 2(a), the particle size distribution has no mono dispersion. The ultrasonic homogenization process was applied to the methanol-based suspension to disperse the agglomerated particles (figure 2(b)). It was found that the particle size distribution shifted to nearly 60 nm. The figure 2(c) TEM images show that the primary particles are changed between 20 and 30 nm for 35A powder. Also, silver is homogeneously dispersed in ABT powders. From the image, residual silver is not observed in powder. The elemental analyses of calculated and experimental silver content in ABT powder are compared in figure 2(d). As shown in the EDX

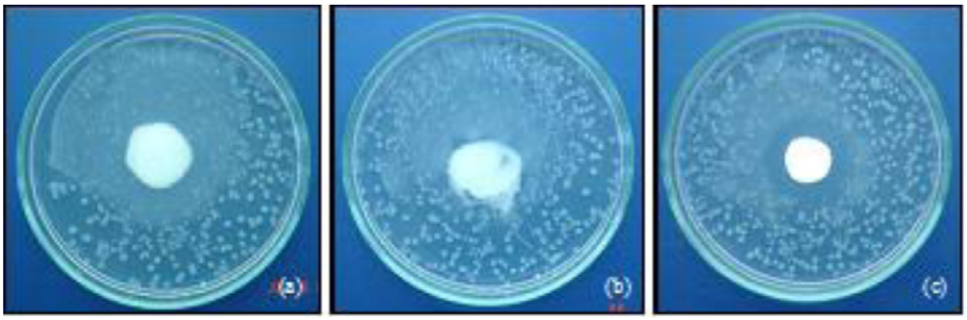

Figure 4. Halo test results for reference and antimicrobial powders: (a) 00A; (b) 10A; and (c) 35A.

analyses, experimental amounts of silver are very close to calculated silver content. The SEM image confirms the particle size distribution results (figure 3). Agglomeration, which has islands of nanoparticles, is observed after synthesis. The XRD chart shows no peak for elemental silver. We may conclude that the silver is in ionic form in the ABT structure. In the TEM analysis, a small cluster of silver has been observed in the nano structure. However, because of its extremely small percentage, which is lower than the detection limit, it cannot be detected by x-ray diffraction. Supporting results for the current investigation have been reported in the literature [32, 33].

Gram-positive *S. aureus*, *P. aeruginosa*, Gram-negative *E.coli*, and yeast were used as the test microorganisms, because they are very common causes of infection in humans. *S. aureus* was specifically selected for this study because it is a part of normal skin flora and it is the most common organism causing implant-related infections. The results of the halo test method are shown in figure 4. Although there was no antibacterial activity observed in the reference powder, an increase in silver content in the powder led to a decrease in the number of bacterial colonies. In the agar dilution test, the reference powder was not effective in bacteria and fungi. However, 20 A and 35 A were effective in bacteria and fungi in each concentration as shown in table 1.

Silver doped calcium phosphate-based inorganic powders were tested for *in vitro* cytotoxicity against V79 379A, NIH-3T3, TIG-114, and HUVEC lines. Dose-dependent cytotoxicity curves, as quantified by the MTT assay for 1, 2, 3, and/or 4 d of exposure of powder on cells are shown in figures 5(a)–(j). This qualitative enzyme assay produced a colored product that was quantified in a microplate reader at a wavelength of 570 nm. According to the MTT results, cell viability was very close to control group on the V79 379A cell line at a concentration of 10 µg/ml for silver content of all powders. Similarly, there was no sharp decrease in cell viability at a concentration of 100 μg ml^{-1} of 5A and 10A content on the V79 379A cell line, whereas the concentration of 20A reduced the cell viability by approximately 30%. At the highest silver content of ABT (35A) at the 100 μg ml^{-1} concentration, cell viability decreased approximately 38% on the first day and 50% on the second, third, and fourth days. ABT showed a sharp increase in the cytotoxicity at the highest tested concentration. The relative growth ratios of V79 379A cells sharply decreased at a concentration of 1000 μg ml^{-1} for 20A and 35A. Doses from 1000 μg ml^{-1} of 20A and 35A were cytotoxic even after the first day after exposure to the cells. However, results of the MTT assay indicate that ABT showed low cytotoxicity against TIG-114 fibroblasts in which the cell viabilities remained 88% at 1000 μg ml^{-1} of 20A (figures 5(h)–(j)). After we incubated the cells with 35A (1000 μg ml^{-1}) for 24 h, the toxicity was approximately 50%. At higher ABT concentrations of all different silver contents, the toxicity values did not differ significantly among various doses on TIG-114 fibroblasts after 24 h. The result of the MTT assay showed that the powder has low cytotoxicity on V79 379A after 4 d of exposure. The 10 μg ml^{-1} and 100 μg ml^{-1} concentrations of ABT and 24 h exposure time was chosen as for the NIH-3T3 and HUVEC MTT assay because only the 1000 μg ml^{-1} concentration of 35 A killed the cells after 24 h exposure. However, depending on the cells used, the effect of the biomaterial on the proliferation rate may be quite different. Several studies demonstrated that the cytotoxicity of a nanomaterial is cell-specific [35, 36]. We observed a significant effect on the proliferation of NIH-3T3 fibroblast cell line at the 10 μg ml^{-1} and 100 μg ml concentrations (figures 5(d) and (e)). However, cell viability decreased approximately 34% at the 10 μg ml^{-1} concentration of 35A (highest silver content of ABT) on the HUVEC line (figure 5(f)). At the 100 μg ml^{-1} concentration of 35A cell viability decreased approximately 50%, although this was the highest concentration of powder (figure 5(g)).

Figure 6 demonstrates representative JC-1 stains of non-apoptotic cells. ABT did not induce the collapse of mitochondrial membrane potential characteristic of apoptotic cells at the 35A concentrations of 10 and 100 μg ml^{-1}, but mitochondrial membrane potential changed after treatment with the 1000 μg ml^{-1} concentration of 35A. This indicates that apoptosis might be the major mechanism of the highest concentration of ABT-mediated toxicity.

Additionally, figure 7 illustrates non-apoptotic nuclei after the treatment of different concentrations of ABT. Cells appear with regular contours and are round

Table 1. Agar dilution test results for 05A, 10A, 20A, and 35A.

	05A						10A						20A						35A					
	%10	%5	%2.5	%1.25	%0.625	%0.3125	%10	%5	%2.5	%1.25	%0.625	%0.3125	% 10	%5	% 2.5	%1.25	%0.625	%0.3125	%10	%5	%2.5	%1.25	%0.625	%0.3125
P. Seudomonas aeruginosa 24 h	−	−	−	+	+	+	−	−	−	−	+	+	−	−	−	−	−	−	−	−	−	−	−	−
P. aeruginosa 48 h	−	−	−	+	+	+	−	−	−	−	+	+	−	−	−	−	−	+	−	−	−	−	−	−
E. coli 24 h	−	−	−	+	+	+	-	−	−	−	−	+	−	−	−	−	−	+	−	−	−	−	−	−
E. coli 48 h	−	−	−	+	+	+	−	−	−	−	+	+	−	−	−	−	−	+	−	−	−	−	−	−
S. aureus 24 h	−	−	−	+	+	+	−	−	−	−	−	+	−	−	−	−	−	+	−	−	−	−	−	−
S. aureus 48 h	−	−	−	+	+	+	−	−	−	−	+	+	−	−	−	−	−	+	−	−	−	−	−	−
C. albicans 24 h	−	−	−	−	+	+	−	−	−	−	−	−	−	−	−	−	−	−	−	−	−	−	−	−
C. albicans 48 h	−	−	−	−	+	+	−	−	−	−	−	−	−	−	−	−	−	−	−	−	−	−	−	−

+, bacteria growth; − , no bacteria growth.

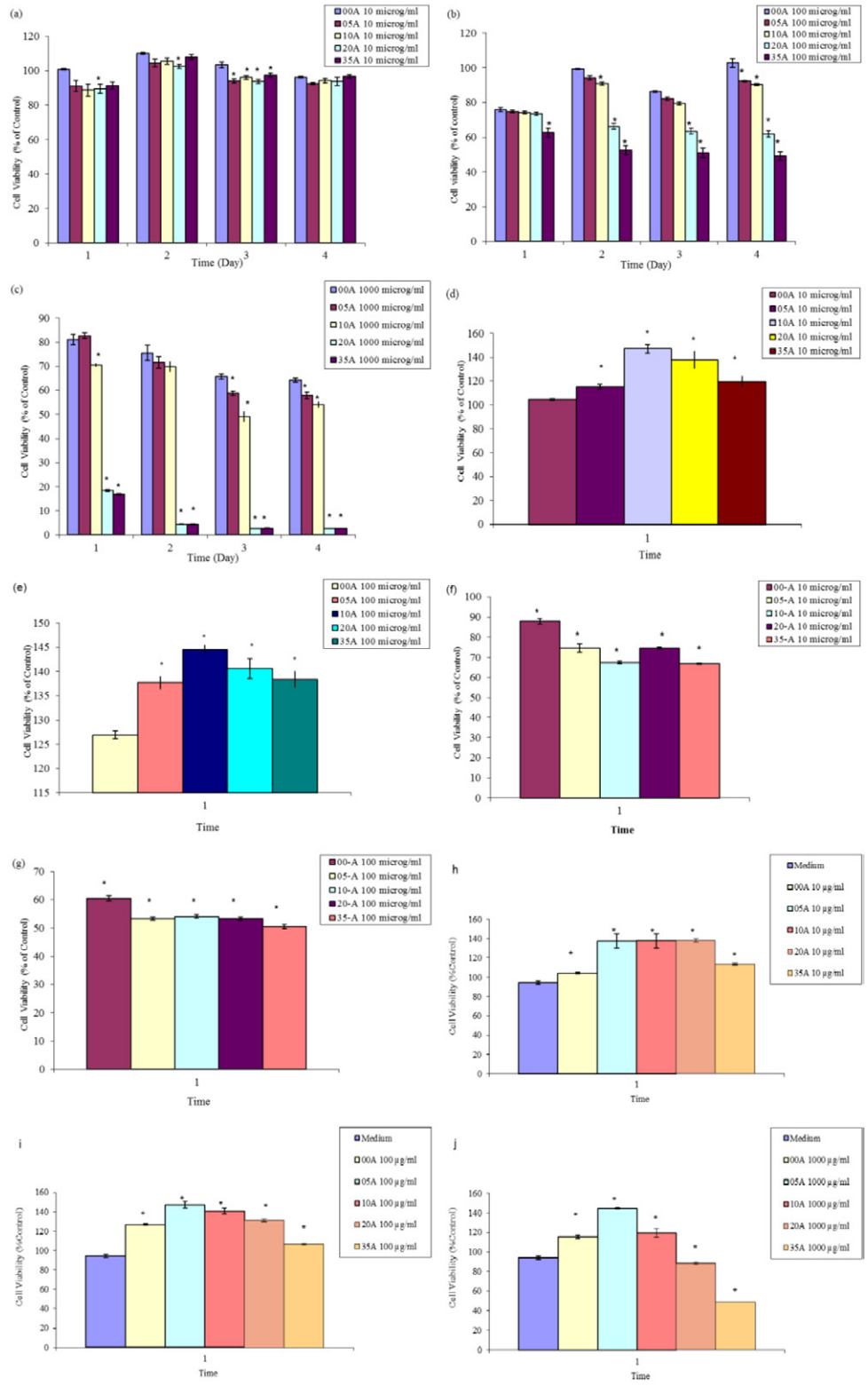

Figure 5. Effects of ABT on the viability of V79 379 (a)–(c), NIH-3T3 (d), (e), HUVEC (f), (g), and TIG-114 (h)–(j) cells. Dose-dependent cytotoxicity curves of MTT assays performed with 1, 2, 3, and 4 d of exposure. The results are expressed as the mean ± SD. *Significant difference from the control group by the Tukey test ($p < 0.05$).

and large. TIG-114 cells with smaller nuclei and condensed chromatin were rarely seen.

The image analyses demonstrated that there was no significant depolarization of F-actin stress fibers after the incubation of 100 μg ml^{-1} concentration of 05A, 10A, and 20A. After 12 h of culture with various doses of ABT containing silver, F-actin stress fibers were slowly disturbed mainly near the edge of pseudopodia-like structures and formed poor fiber bundles of stress fiber in a dose-dependent manner (figure 8).

In the *in vitro* wound healing assay, a defined 'wound' was scraped across TIG-114 fibroblasts. The data showed that in all of the examined concentrations (10, 100, and 1000 μg ml^{-1}) and especially at 10 μg ml^{-1}

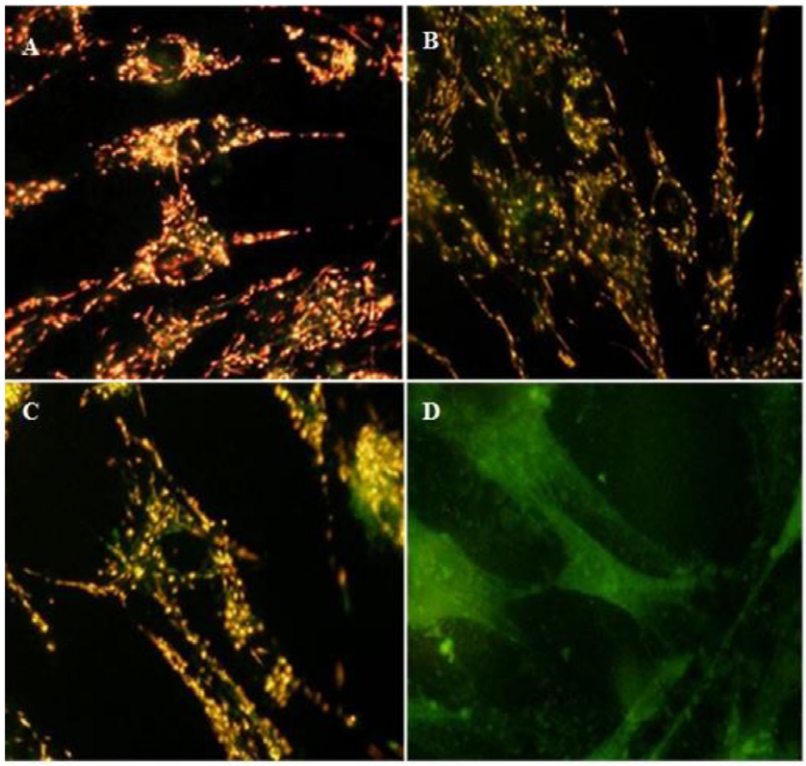

Figure 6. The effects of 35A on mitochondrial membrane potential in TIG-114 cells were assessed by fluorescence staining with JC-1, exist as a monomer in the cytosol (green), and accumulate as aggregates in the mitochondria, which appear red/orange in non-apoptotic cells. (a) Control. (b) 10 μg ml^{-1}. (c) 100 μg ml^{-1}. (d) 1000 μg ml^{-1}. Images were taken using an objective lens of 20X.

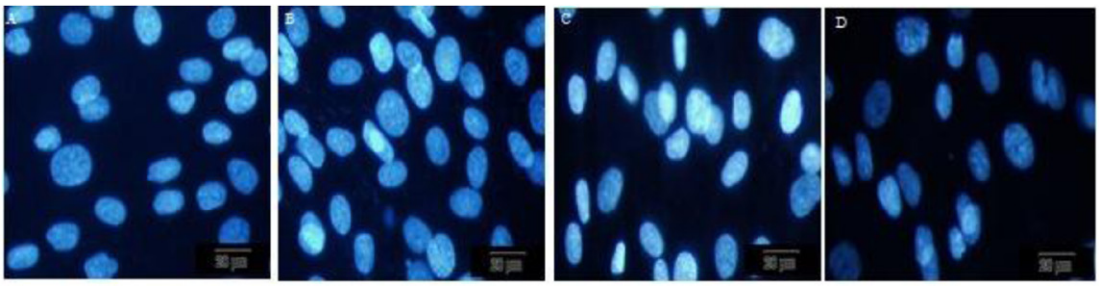

Figure 7. The effect of 05A on apoptosis detection in TIG-114 cells was assessed by fluorescence staining with DAPI, a substance that specifically binds DNA. (a) Control cells and (b) 10 μg ml^{-1}, (c) 100 μg ml^{-1}, and (d) 1000 μg ml^{-1}. Scale bar, 20 μM.

(figure 9(b)) 35A (highest silver concentration of ABT) showed an obvious increase in the rate of wound closure, noted at 12 h (figure 9).

We investigated the angiogenic potential of silver containing calcium phosphate-based ceramic powder on HUVECs because endothelial cells are key cells in angiogenesis. Based on the previous results, two dilutions (10 μg ml^{-1} and 100 μg ml^{-1} of 35A) were chosen for the tube formation assay. In the control, 10 μg ml^{-1} and 100 μg ml^{-1} dilutions of 35A groups, HUVECs on a matrigel substratum displayed high motility and differentiated into well-defined network-like structures within 12 h (figures 10(a)–(c)). The 10 μg ml^{-1} and 100 μg ml^{-1} dilutions of 35A could stimulate HUVEC tube formation in a dose-dependent manner.

Therefore, it can be concluded that the ABT (or PAG) exhibits good biocompability at lower concentrations (10 μg ml^{-1} and 100 μg ml^{-1}), with a high silver content, which makes it suitable for biomedical applications.

4. Discussion

The degradation of implanted ceramics permits the bone to grow into the implanted tissue, providing eventual replacement for the natural tissue environment. Due to their flawless biocompatibility and their structural similarities to natural bone, calcium phosphate–based materials have attracted the most attention [35]. Both the nature and the degree of tissue response are dependent on various characteristics of the material, such as its chemical composition [36], surface texture [37], porosity, density [38], shape, and size [39].

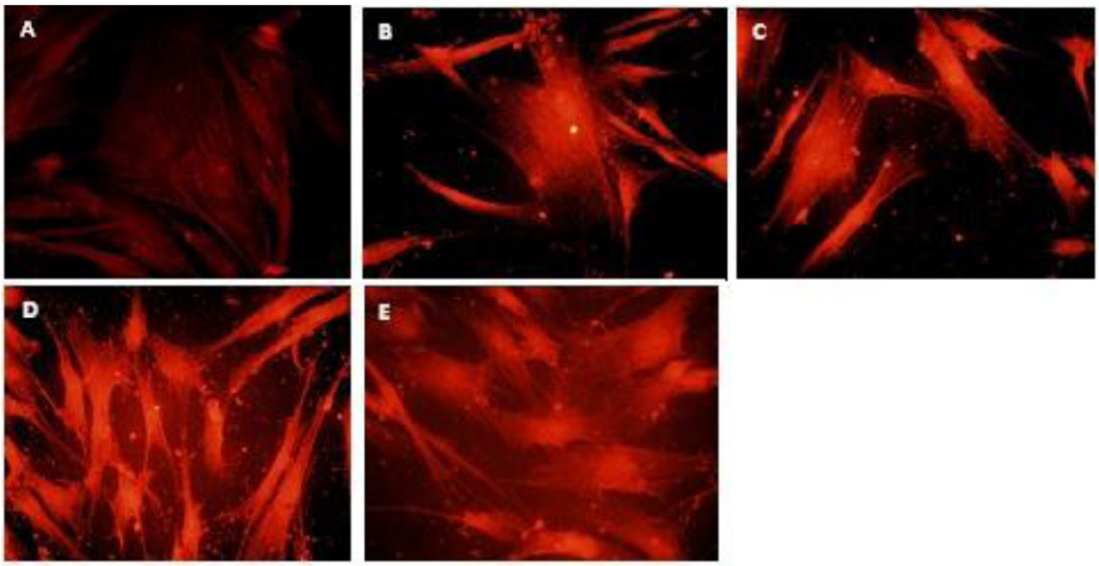

Figure 8. The effect of ABT on actin stress-fiber polymerization in TIG-114 cells was assessed by fluorescence staining with TRITC phalloidin, a substance that specifically detects F-actin. (a) Control; TIG-114 cells were treated with 100 μg ml^{-1} of (b) 05A; (c) 10A; (d) 20A; and (e) 35A. Images were taken using an objective lens of 20X.

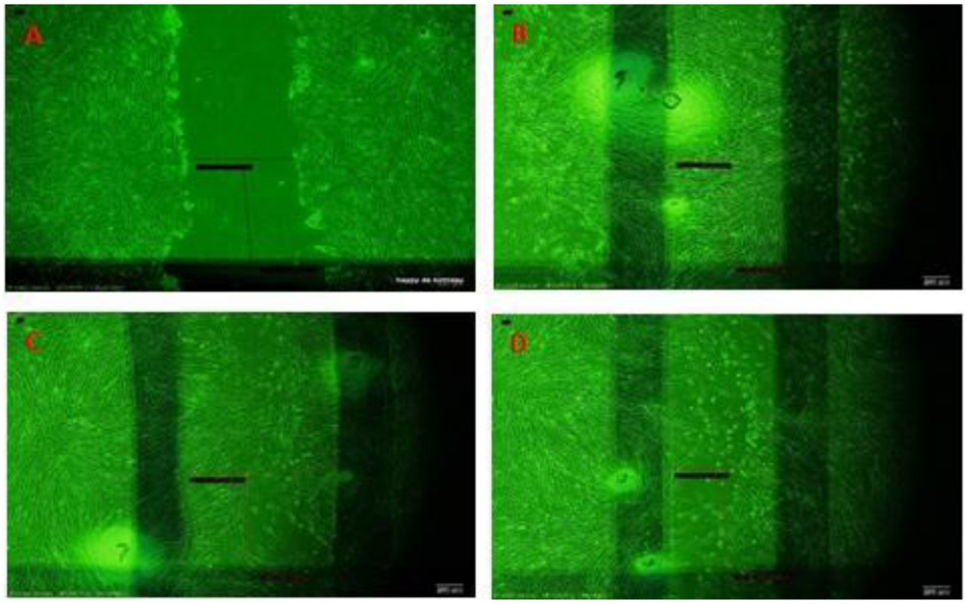

Figure 9. Effect of 35A on cell migration. (a) Wounded cells; TIG-114 cells were treated with (b) 10 μg ml^{-1} and (c) 100 μg ml^{-1} and 1000 μg ml^{-1}. Cells were incubated with various concentrations of ABT, and cell migration was examined at 12 h after treatment by wound healing (A). Scale bar, 100 μm.

There are several biomaterial surface treatments for the reduction of implant-associated infections. Surface functionalization techniques constitute the core of previous work, focusing on treating antibacterial characteristics with biomaterials. These techniques include a variety of procedures, namely covalently attaching polycationic groups [40, 41], impregnating or loading chitosan nanoparticles with antibacterial agents [42–44], and coating of implant surfaces with quaternary ammonium compounds, iodine, or Ag^{+} ions [45–47]. Cell cultures techniques are well-established and highly reproducible, and have been used to assess silver toxicity. The density, morphology, and the viability of the cells differ according to the surface reactivity and physico-chemical nature of the substrate [48]. In the present study, JC-1 and DAPI staining were applied to TIG-114 cells. Mitochondria perform a variety of biochemical processes, including oxidative phosphorylation, which provides most of the energy for the cell. Mitochondrial oxidative phosphorylation is dependent on a proton electrochemical gradient ($\Delta\Psi$m) generated by respiration and maintained by the impermeability of the inner membrane to protons. If the mitochondrial membrane is rendered permeable to protons, the membrane potential dissipates. The distinguishing trademark for apoptosis is the loss of mitochondrial mem-

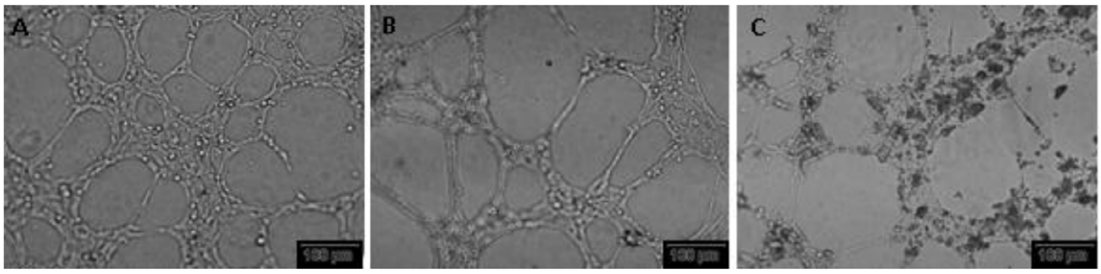

Figure 10. Angiogenic effects of the highest doses of ABT on HUVECs. (a) Control cells. (b) HUVECs were treated with powder 35A at a concentration of 10 μg ml^{-1} of (c) 35A at a concentration of 100 μg ml^{-1}. HUVECs were cultured on matrigel matrix and incubated with 10 μg ml^{-1} and 100 μg ml^{-1} concentrations of all powders, and capillary-like tube formation was examined at 12 h after treatment. Scale bar, 100 μm.

brane potential, which is an early event that happens to be coinciding with caspase activation. JC-1 exists in the cytosol as a monomer that emits a green fluorescence and accumulates in the mitochondria as piles that emit an orange-red fluorescence in non-apoptotic cells [49–51]. DAPI staining is another method to determine apoptotic effects of test materials. It is a substance that specifically binds DNA and shows degradation of DNA into fragments.

To provide an illustrative example, the interaction of silver with cellular energy production can be used. Because the location of the essential protein complexes of the bacterial electron transportation chain happens to be on the cell exterior, it is relatively easy for the reactive silver ions to access and to inactivate. Contrarily, the same structures are located intracellularly in the mitochondrial organelles in eukaryotic cells. To both penetrate the cellular membrane, which acts as a diffusion barrier, and to have comparable inactivation of mitochondrial proteins, higher silver concentrations are needed. In addition to this, although eukaryotic cells regularly contain several mitochondria, bacterial cells do not have that sort of abundance to protect their biological energy conservation system from the assault of silver ions. Therefore, although bacterial respiration is already being seriously encumbered, eukaryotic cell respiration remains unblocked [52]. In this study it was observed that increasing silver content in powder led to a decrease of bacterial activity, an increase in the cytotoxicity of V79 379A and HUVEC cell lines, and an increase in the proliferation of NIH-3T3 and TIG-114 cells.

Angiogenesis is crucial for both bone tissue regeneration and bone tissue engineering. Angiogenic induction by bone material itself is not only a simple approach but also an effective neovascularization approach [53–56]. Endothelial cells, which take part in the construction of the microvasculature that provides oxygen and nutrients supply along with waste elimination, are the primary cells involved in angiogenesis [57, 58]. For the process of angiogenesis to occur normally, both proliferation and migration are required [59]. Migration is a key step required for angiogenesis in both endothelial cells and fibroblasts. Additionally, actin rearrangement is an important event in the attachment capability and cell migration. To determine the effects of ABT on cell migration and attachment, fluorescent phalloidin stain, which binds specifically at the interface between F-actin subunits [60], and a wound healing assay were used. Clarifying the process of vascularization and its mechanism is of great significance for design and development of medical biomaterials. In this area, it is noted that the endothelial tubes of new capillaries are formed by intracellular vacuoles, which has been demonstrated in an *in vitro* model of angiogenesis [61]. We used HUVECs as one of the common endothelial reference cell types [62]. Fibroblasts enhance micro vessel formation, development, and maturation [63]. Fibroblasts were found to stabilize endothelial cell-lined tube formation [64] and provide important signaling that leads to the maturation of capillaries made of HUVECs. In the present study three fibroblast cell lines and an endothelial cell line were used to investigate the cytotoxic and proliferative activities of silver doped calcium phosphate-based ceramic nano powder. The neo-vascularization of the host site is crucial for the primary fixation and the long-term stability of the bone-implant interface [58]. In the later stages of angiogenesis, endothelial cells have to rearrange themselves into a tube to form a new small blood vessel. Thus, the endothelial cell tube formation assay used here is an *in vitro* model of this process. In the present study we revealed that 10 μg ml^{-1} and 100 μg ml^{-1} concentrations of the highest metal ion content of silver doped calcium phosphate-based inorganic powder (35A) did not disrupt the tube formation of HUVECs.

In contrast to our findings, there have been reports showing that silver nanoparticles can inhibit tube formation of endothelial cells [65–67]; however, Kang *et al* [68] revealed that silver nanoparticles can cause angiogenesis through the production of angiogenic factors.

Particle size analysis of synthesized silver doped HAP powders (ABT or PAG) exhibited that the powder has monomodal size distribution without dissolution of silver to form a cluster at low percentages. However, a small cluster formation is observed for higher silver contents. Also, particle size of a silver cluster is less than 3 nm. TEM images confirm that it is homogeneously distributed in calcium phosphate particles. If powder contains silver particles, then two peaks between 1 and

3 nm and 20 and 100 nm from size distributions plot are expected. However, as seen in figure 2(b), there is one peak between 40 and 100 nm (nano particle agglomeration) due to the electrostatic forces between nanoparticles. To summarize, we suggest that calcium phosphate is a good carrier for silver without any dissolution in HAP structure.

Amazingly, silver in the HAP diffuses inside the biological environment very slowly, and thus the silver content shows antimicrobial activity without causing toxic effect on mammalian cells.

5. Conclusion

In this study, silver doped nanosize calcium phosphate-based powder possesses a very strong antibacterial influence against *E. coli*, *P. aeruginosa*, *S. aureus*, and *C. albicans* with increasing silver content. Antibacterial powders showed a concentration-dependent cytotoxicity on V79 379A and HUVEC lines. Although a low concentration of 100 μg ml^{-1} powder is not cytotoxic on the V79 379A cell line, increases in silver concentration gradually increases the cytotoxicity of the powder. However, antibacterial powders stimulated proliferation of NIH-3T3 and TIG-114 cell lines. In addition, antibacterial powders exerted an angiogenic potential. We demonstrated, for the first time, that silver doped calcium phosphate-based ceramic nano powder does not disturb angiogenesis *in vitro* at a concentration of 100 μg ml^{-1} of 35A with the highest silver content. As demonstrated by JC-1 and DAPI staining and wound healing assay, we conclude that ABT is non-cytotoxic and bears good biocompability even at 1000 μg ml^{-1} of ABT with the highest content of silver. F-actin staining results show that ABT (or PAG) has good attachment ability, but high doses of 35A caused f-actin depolimerization. Consequently, the silver doped calcium phosphate-based ceramic nano powder can be used in implant materials as a coating material, and these coated implants may prevent bacterial colonization as compared to uncoated implants.

Acknowledgments

The authors are grateful to Anadolu University, Commission of Scientific Research Projects (Projects 050210 and 080246), Scientific and Technological Research Council of Turkey (TUBITAK-108M177), Republic of Turkey-Ministry of Industry (SAN-TEZ 0086.STZ.2007-1) for financial support. The authors also sincerely thank Caitrin Crudden (Karolinska Institute, Department of Oncology-Pathology, Cancer Center Karolinska) for proofreading of manuscript.

References

[1] Ignjatovic N *et al* 2006 Cytotoxicity and fibroblast properties during *in vitro* test of biphasic calcium phosphate/poly-dl-lactide-co-glycolide biocomposites and different phosphate materials *Microsc. Res. Tech.* **69** 976–82

[2] Simon C G, Antonucci J M, Liu D W and Skptic D 2005 *In vitro* cytotoxicity of amorphous calcium phosphate composites *J. Bioact. Compat. Pol.* **20** 279–95

[3] Organization IS 2014 Biological evaluation of medical devices, part 5: test for *in vitro* cytotoxicity, ISO 10993–5 [cited 06.04.2014]; available from: www.iso.org/iso/catalogue_detail.htm?csnumber=36406

[4] Rosenstiel P, Lucius R, Deuschl G, Sievers J and Wilms H 2001 From theory to therapy: implications from an *in vitro* model of ramified microglia *Microsc. Res. Tech.* **54** 18–25

[5] Novosel E C, Kleinhans C and Kluger P J 2011 Vascularization is the key challenge in tissue engineering *Adv. Drug Deliv. Rev.* **63** 300–11

[6] Anderson S M, Siegman S N and Segura T 2011 The effect of vascular endothelial growth factor (VEGF) presentation within fibrin matrices on endothelial cell branching *Biomaterials* **32** 7432–43

[7] Bose S and Tarafder S 2012 Calcium phosphate ceramic systems in growth factor and drug delivery for bone tissue engineering: a review *Acta Biomater.* **8** 1401–21

[8] Hankenson K D, Dishowitz M, Gray C and Schenker M 2011 Angiogenesis in bone regeneration *Injury* **42** 556–61

[9] Tang H Q, Liu T, Liu X, Gu H Q and Zhao J 2007 A study on biocompatibility and bactericidal properties of pyrolytic carbon by silver ion implantation *Nucl. Instrum. Methods Phys. Res.* B **255** 304–8

[10] Zhang F, Wolf G K, Wang X and Liu X 2001 Surface properties of silver doped titanium oxide films *Surf. Coat. Technol.* **148** 65–70

[11] Atiyeh B S, Costagliola M, Hayek S N and Dibo S A 2007 Effect of silver on burn wound infection control and healing: review of the literature *Burns* **33** 139–48

[12] Heggers J P *et al* 2002 Acticoat versus silverlon: the truth: 150 *J. Burn Care Res.* **23** S115

[13] Russell A D and Hugo W B 1994 Antimicrobial activity and action of silver *Prog. Med. Chem.* **31** 351–70

[14] Fan F-R F and Bard A J 2001 Chemical, electrochemical, gravimetric, and microscopic studies on antimicrobial silver films *J. Phys. Chem.* B **106** 279–87

[15] Mirsattari S M, Hammond R R, Sharpe M D, Leung F Y and Young G B 2004 Myoclonic status epilepticus following repeated oral ingestion of colloidal silver *Neurology* **62** 1408–10

[16] Hangst K, Eitenmüller J, Weltin R and Peters G 1987 Hydroxylapatite silver phosphate ceramics: production, analysis and biological testing of their antibacterial effectiveness *MRS Online Proc. Library* 110

[17] Kim T N *et al* 1998 Antimicrobial effects of metal ions (Ag^{+}, Cu^{2+}, Zn^{2+}) in hydroxyapatite *J. Mater. Sci. Mater. Med.* **9** 129–34

[18] Eitenmuller J, Hangst K, Peters G and Golsong W 1989 Tissue tolarence and antibacterial effectiveness of hydroxylapatite silver phosphate ceramics *Mater. Res. Soc. Symp.* 277–84

[19] Trop M, Novak M, Rodl S, Hellbom B, Kroell W and Goessler W 2006 Silver-coated dressing acticoat caused raised liver enzymes and argyria-like symptoms in burn patient *J. Trauma* **60** 648–52

[20] Mooney E K, Lippitt C, Friedman J and Committee PSEFD 2006 Silver dressings *Plast. Reconstr. Surg.* **117** 666–9

[21] Warriner R and Burrell R 2005 Infection and the chronic wound: a focus on silver *Adv. Skin Wound Care* **1** 2–12

[22] Kirsner R S, Orstead H and Wright J B 2001 Matrix metalloproteinases in normal and impaired wound healing: a potential role for nanocrystalline silver *Wounds: A Compend. Clin. Res. Practice* **13** 5–12

[23] Darouiche R O 1999 Anti-infective efficacy of silver-coated medical prostheses. *Clin. Infect. Dis.* **29** 1371–7 quiz 8

[24] Wright J B, Lam K and Burrell R E 1998 Wound management in an era of increasing bacterial antibiotic resistance: a role for topical silver treatment *Am. J. Infect. Control* **26** 572–7

[25] Mosmann T 1983 Rapid colorimetric assay for cellular growth and survival: application to proliferation and cytotoxicity assays *J. Immunol. Methods* **65** 55–63

[26] Bostancıoğlu R B, Koparal A T and Benkli K 2014 Investigation of the pharmacological profiles of dinuclear metal complexes

as novel, potent and selective cytotoxic agents against ras-transformed cells *Environ. Toxicol. Pharmacol.* **37** 897–906
[27] Bostancioglu R B, Kurkcuoglu M, Baser K H C and Koparal A T 2012 Assessment of anti-angiogenic and anti-tumoral potentials of origanum onites L. essential oil *Food Chem. Toxicol.* **50** 2002–8
[28] Rubin L L *et al* 1991 A cell culture model of the blood-brain barrier *J. Cell Biol.* **115** 1725–35
[29] Bostancioglu R B, Demirel S, Cin G T and Koparal A T 2013 Novel ferrocenyl-containing N-acetyl-2-pyrazolines inhibit *in vitro* angiogenesis and human lung cancer growth by interfering with F-actin stress fiber polimeryzation *Drug Chem. Toxicol.* **36** 484–95
[30] Ouchi N *et al* 2004 Adiponectin stimulates angiogenesis by promoting cross-talk between AMP-activated protein kinase and Akt signaling in endothelial cells *J. Biol. Chem.* **279** 1304–9
[31] Costescu A *et al* 2013 Fabrication, characterization, and antimicrobial activity, evaluation of low silver concentrations in silver-doped hydroxyapatite nanoparticles *J. Nanomater.* **2013** 9
[32] Ciobanu C, Massuyeau F, Constantin L and Predoi D 2011 Structural and physical properties of antibacterial Ag-doped nano-hydroxyapatite synthesized at 100 °C *Nanoscale Res Lett.* **6** 613
[33] Ciobanu C S, Iconaru S L, Chifiriuc M C, Costescu A, Le Coustumer P and Predoi D 2013 Synthesis and antimicrobial activity of silver-doped hydroxyapatite nanoparticles *Biomed. Res. Int.* **2013** 10
[34] Rameshbabu N, Sampath Kumar T S, Prabhakar T G, Sastry V S, Murty K V G K and Prasad Rao K 2007 Antibacterial nanosized silver substituted hydroxyapatite: synthesis and characterization *J. Biomed. Mater. Res.* A **80A** 581–91
[35] Seeley Z, Bandyopadhyay A and Bose S 2007 Influence of TiO_2 and Ag_2O addition on tricalcium phosphate ceramics *J. Biomed. Mater. Res.* A **82** 113–21
[36] Klein C P, de Groot K, Driessen A A and van der Lubbe H B 1986 A comparative study of different beta-whitlockite ceramics in rabbit cortical bone with regard to their biodegradation behaviour *Biomaterials* **7** 144–6
[37] Taylor S R and Gibbons D F 1983 Effect of surface texture on the soft tissue response to polymer implants *J. Biomed. Mater. Res.* **17** 205–27
[38] Davila J C, Lautsch E V and Palmer T E 1968 Some physical factors affecting the acceptance of synthetic materials as tissue implants *Ann. New York Acad. Sci.* **146** 138–47
[39] Wood N K, Kaminski E J and Oglesby R J 1970 The significance of implant shape in experimental testing of biological materials: disc versus rod *J. Biomed. Mater. Res.* **4** 1–12
[40] Tiller J C, Liao C-J, Lewis K and Klibanov A M 2001 Designing surfaces that kill bacteria on contact *Proc. Natl Acad. Sci.* **98** 5981–5
[41] Cen L, Neoh K G and Kang E T 2004 Antibacterial activity of cloth functionalized with N-alkylated poly(4-vinylpyridine) *J. Biomed. Mater. Res* A **71** 70–80
[42] van de Belt H, Neut D, Schenk W, van Horn J R, van der Mei H C and Busscher H J 2001 Infection of orthopedic implants and the use of antibiotic-loaded bone cements. A review *Acta Orthop. Scand.* **72** 557–71
[43] Schmidmaier G, Lucke M, Wildemann B, Haas N P and Raschke M 2006 Prophylaxis and treatment of implant-related infections by antibiotic-coated implants: a review *Injury* **37** 105–12
[44] Shi Z, Neoh K G, Kang E T and Wang W 2006 Antibacterial and mechanical properties of bone cement impregnated with chitosan nanoparticles *Biomaterials* **27** 2440–9
[45] Yorganci K, Krepel C, Weigelt J A and Edmiston C E 2002 *In vitro* evaluation of the antibacterial activity of three different central venous catheters against gram-positive bacteria. *Eur. J. Clin. Microbiol. Infect. Dis.* **21** 379–84
[46] Nohr R S and Macdonald J G 1994 New biomaterials through surface segregation phenomenon: new quaternary ammonium compounds as antibacterial agents *J. Biomater. Sci. Polym. Edn* **5** 607–19
[47] Tyagi M and Singh H 1997 Preparation and antibacterial evaluation of urinary balloon catheter *Biomed. Sci. Instrum.* **33** 240–5 (PMID: 9731365)
[48] John A, Varma H K and Kumari T V 2003 Surface reactivity of calcium phosphate based ceramics in a cell culture system *J. Biomater. Appl.* **18** 63–78
[49] Ozalp S S, Eren C Y, Bostancioglu R B and Koparal A T 2012 Induction of apoptosis and inhibition of cell proliferation by the cyclooxgenase enzyme blocker nimesulide in the ishikawa endometrial cancer cell line *Eur. J. Obstet. Gynecol. Reprod. Biol.* **164** 79–84
[50] Castedo M, Ferri K, Roumier T, Metivier D, Zamzami N and Kroemer G 2002 Quantitation of mitochondrial alterations associated with apoptosis *J. Immunol. Methods* **265** 39–47
[51] Sebastian A, Allan E, Allan D, Colthurst J and Bayat A 2011 Addition of novel degenerate electrical waveform stimulation with photodynamic therapy significantly enhances its cytotoxic effect in keloid fibroblasts: first report of a potential combination therapy *J. Dermatol. Sci.* **64** 174–84
[52] Alt V *et al* 2004 An *in vitro* assessment of the antibacterial properties and cytotoxicity of nanoparticulate silver bone cement *Biomaterials* **25** 4383–91
[53] Kanczler J M and Oreffo R O 2008 Osteogenesis and angiogenesis: the potential for engineering bone *Eur. Cells Mater.* **15** 100–14 (PMID: 18454418)
[54] Gorustovich A A, Roether J A and Boccaccini A R 2010 Effect of bioactive glasses on angiogenesis: a review of *in vitro* and *in vivo* evidences *Tissue Eng.* B **16** 199–207
[55] Mooney D 2008 Materials for angiogenesis on demand *Eur. Cells Mater.* **16** 17
[56] Zhai W *et al* 2012 Silicate bioceramics induce angiogenesis during bone regeneration *Acta Biomater.* **8** 341–9
[57] Peters K, Unger R E, Brunner J and Kirkpatrick C J 2003 Molecular basis of endothelial dysfunction in sepsis *Cardiovasc. Res.* **60** 49–57
[58] Khalil G, Lorthois S, Marcoux M, Mansat P and Swider P 2011 Wave front migration of endothelial cells in a bone-implant interface *J. Biomech.* **44** 1980–6
[59] Krill D, Madden J, Huncik K and Moeller P D 2010 Induced thyme product prevents VEGF-induced migration in human umbilical vein endothelial cells *Biochem. Biophys. Res. Commun.* **403** 275–81
[60] Sangani R *et al* 2014 Knockdown of SVCT2 impairs *in vitro* cell attachment, migration and wound healing in bone marrow stromal cells *Stem Cell Res.* **12** 354–63
[61] Bai L, Zhan K, Hu Q and Xu J 2014 Endothelial tubes form from intracellular vacuoles in implanted biomaterial *in vivo* of rat *J. Mater. Sci. Mater. Med.* **25** 1275–82
[62] Bondar B, Fuchs S, Motta A, Migliaresi C and Kirkpatrick C J 2008 Functionality of endothelial cells on silk fibroin nets: comparative study of micro- and nanometric fibre size *Biomaterials* **29** 561–72
[63] Sukmana I and Vermette P 2010 The effects of co-culture with fibroblasts and angiogenic growth factors on microvascular maturation and multi-cellular lumen formation in HUVEC-oriented polymer fibre constructs *Biomaterials* **31** 5091–9
[64] Armulik A, Abramsson A and Betsholtz C 2005 Endothelial/pericyte interactions *Circ. Res.* **97** 512–23
[65] Gurunathan S, Lee K J, Kalishwaralal K, Sheikpranbabu S, Vaidyanathan R and Eom S H 2009 Antiangiogenic properties of silver nanoparticles *Biomaterials* **30** 6341–50
[66] Kemp M M *et al* 2009 Gold and silver nanoparticles conjugated with heparin derivative possess anti-angiogenesis properties *Nanotechnology* **20** 455104
[67] Sheikpranbabu S, Kalishwaralal K, Venkataraman D, Eom SH, Park J and Gurunathan S 2009 Silver nanoparticles inhibit VEGF-and IL-1beta-induced vascular permeability via Src dependent pathway in porcine retinal endothelial cells *J. Nanobiotechnol.* **7** 8
[68] Kang K *et al* 2011 Vascular tube formation and angiogenesis induced by polyvinylpyrrolidone-coated silver nanoparticles *Toxicol. Lett.* **205** 227–34